Tellus (2003), 55B, 530–546
Printed in UK. All rights reserved

TELLUS
ISSN 0280–6509

Inter-annual variability of the atmospheric carbon dioxide concentrations as simulated with global terrestrial biosphere models and an atmospheric transport model

By DAISUKE FUJITA[1†], MISA ISHIZAWA[2*], SHAMIL MAKSYUTOV[2], PETER E. THORNTON[3], TAZU SAEKI[1§] and TAKAKIYO NAKAZAWA[1,2], [1]*Center for Atmospheric and Oceanic Studies, Graduate School of Science, Tohoku University, Sendai 980-8578, Japan;* [2]*Frontier Research System for Global Change, Institute for Global Change Research, 3173-25 Showa-machi, Kanazawa-ku, Yokohama 236-0001, Japan;* [3]*Climate and Global Dynamics Division, National Center for Atmospheric Research, P.O. Box 3000, Boulder, CO 80307, USA*

(Manuscript received 21 January 2002; in final form 18 November 2002)

ABSTRACT

Seasonal and inter-annual variations of atmospheric CO_2 for the period from 1961 to 1997 have been simulated using a global tracer transport model driven by a new version of the Biome BioGeochemical Cycle model (Biome-BGC). Biome-BGC was forced by daily temperature and precipitation from the NCEP reanalysis dataset, and the calculated monthly-averaged CO_2 fluxes were used as input to the global transport model. Results from an inter-comparison with the Carnegie–Ames–Stanford Approach model (CASA) and the Simulation model of Carbon cYCle in Land Ecosystems (Sim-CYCLE) model are also reported. The phase of the seasonal cycle in the Northern Hemisphere was reproduced generally well by Biome-BGC, although the amplitude was smaller compared to the observations and to the other biosphere models. The CO_2 time series simulated by Biome-BGC were compared to the global CO_2 concentration anomalies from the observations at Mauna Loa and the South Pole. The modeled concentration anomalies matched the phase of the inter-annual variations in the atmospheric CO_2 observations; however, the modeled amplitude was lower than the observed value in several cases. The result suggests that a significant part of the inter-annual variability in the global carbon cycle can be accounted for by the terrestrial biosphere models. Simulations performed with another climate-based model, Sim-CYCLE, produced a larger amplitude of inter-annual variability in atmospheric CO_2, making the amplitude closer to the observed range, but with a more visible phase mismatch in a number of time periods. This may indicate the need to increase the Biome-BGC model sensitivity to seasonal and inter-annual changes in temperature and precipitation.

1. Introduction

Measurements of atmospheric CO_2 show that about half of CO_2 emissions from fossil-fuel burning remain in the atmosphere, and that there is substantial inter-annual variability in the rate of atmospheric CO_2 accumulation, due to changes in the CO_2 exchange between the atmosphere and the other main carbon reservoirs of the terrestrial biosphere and the oceans. To study such observed variability, a number of investigations have been carried out. For example, inverse calculations using atmospheric CO_2 measurements and corresponding isotope ratios enable us to separate the uptake of anthropogenic CO_2 between the terrestrial biosphere and the oceans (Keeling et al., 1995; Francey et al.,

*Corresponding author.
e-mail: misa@jamstec.go.jp
†Present affiliation: NEC Software Inc, Shinkiba Center Building, 1-18-6 Shinkiba, Koto-ku, Tokyo 136-8608, Japan.
§Present affiliation: Research Institute for Humanity and Nature, 335 Takashima-cho, Kamigyo-ku, Kyoto 602-0878, Japan.

1995; Morimoto et al., 2000), but they can not explain the underlying mechanisms and processes which cause the anomalies of carbon fluxes.

As a result of those inverse modeling studies, the terrestrial biosphere has been recognized to play an important role in the variability and future levels of atmospheric CO_2 concentration as affected by climatic variability and other environmental changes. This recognition has encouraged the development of terrestrial biosphere models (TBM) to elucidate the processes of terrestrial ecosystems related to the observed anomalies of atmospheric CO_2 concentration, as shown by some recent studies (e.g., Heimann et al., 1998). Each ecosystem model has been developed for a specific purpose, with different formulations of plant physiological processes. Existing models are diverse with respect to structure and characteristics, but they can be categorized mainly into two main types. One type is driven by satellite vegetation data, i.e., the normalized difference vegetation index (NDVI) from the Advanced Very High Resolution Radiometer (AVHRR). These models range from simple models with no physiological mechanics (e.g. Fung et al., 1987) to more comprehensive models with a number of parameterized mechanistic formulations (e.g. Randerson et al., 1997). NDVI-based models have an advantage of reflecting the observed temporal and spatial patterns of biospheric activities, but their application is limited only to the recent period when satellite data are available. The other type is a process-based model, which uses only climatic data and other environmental parameters, and has mechanistic functions of phenology responding to the environment. The main advantage of this type of model is that it can be used for predicting the atmospheric CO_2 level in the past and the future, as long as the necessary environmental data are provided.

The objective of this paper is to investigate the extent to which climate-driven anomalies in simulated terrestrial biospheric CO_2 fluxes can explain the observed inter-annual variations in atmospheric CO_2. For this purpose, we implemented a single point process-based ecosystem model, Biome-BGC (Thornton, 1998; Thornton et al., 2002) for a global terrestrial carbon cycle simulation. Firstly, to evaluate the model performance of Biome-BGC, we simulated the atmospheric seasonal CO_2 cycle by an off-line coupling of Biome-BGC to a three-dimensional atmospheric tracer transport model. The results were then compared with the observed atmospheric CO_2 and two other global net ecosystem production (NEP) datasets obtained by the Simulation model of Carbon cYCle in Land Ecosystems (Sim-CYCLE, Ito and Oikawa, 2000) and the Carnegie–Ames–Stanford Approach model (CASA, Randerson et al., 1996). Sim-CYCLE is another process-based model driven by environmental parameters. On the other hand, CASA is a satellite-based model. Hunt et al. (1996) conducted a global simulation using a previous version of Biome-BGC. A major improvement in the present version of the model is that it does not require satellite observations. Inter-comparison results have been reported by Nemry et al. (1999), in which Biome-BGC was driven by climatological monthly data, while the daily data from the NCEP reanalysis were used to drive Biome-BGC in the present study. Secondly, we estimated inter-annual variability in NEP for the period from 1961 to 1997 by Biome-BGC, and compared the predicted global anomalies of atmospheric CO_2 with those obtained from historical observation records and from the other modeled fluxes by Sim-CYCLE. The Carbon Cycle Model Linkage Project (CCMLP) conducted long-term global simulations of four process-based biosphere models, taking into account the atmospheric CO_2 increase and cropland usage, along with climate variability. Focusing on the conjunct effects of these three factors on the terrestrial carbon storage between 1920 and 1992, their model analyses indicated that the long-term climate variations have a much smaller effect on terrestrial carbon storage than the increasing atmospheric CO_2, but the sensitivity of carbon storage to climate variability is still one of the main uncertainties (McGuire et al., 2001). In this study we forced the calculation on the climate-driven inter-annual anomalies of carbon exchange between the atmosphere and the terrestrial biosphere with the daily climate dataset.

2. Model and data descriptions

2.1. Terrestrial biospheric CO_2 fluxes

We employed Biome-BGC for estimating global NEP. Also we examined two other model estimates of net biospheric CO_2 fluxes for comparison with those of Biome-BGC: Sim-CYCLE (Ito and Oikawa, 2000), and CASA (Randerson et al., 1996). Biome-BGC and Sim-CYCLE are both process-based models that rely upon empirical phonological patterns driven by seasonal changes in temperature and precipitation, while CASA uses satellite data to do so. The detailed descriptions of all three models have been presented

elsewhere (Thornton, 1998; Running and Hunt, 1993; Ito and Oikawa, 2000; Potter et al., 1993; Randerson et al., 1996). In the following subsections, we briefly describe the global simulation with Biome-BGC and each of the three model structures.

2.1.1. Biome-BGC. The Biome-BGC model was originally developed as a single-point model, FOREST-BGC (Running and Coughlan, 1988; Running and Hunt, 1993), to simulate a forest ecosystem development. It has been improved by validation with different ecosystems and now includes nitrogen cycling and hydrological processes (Nemani and Running, 1989; Running, 1994). We used the Biome-BGC model version 4.1.1 (Thornton, 1998; Thornton et al., 2002)for a global terrestrial biosphere simulation, following the approach of Hunt et al. (1996). The latter study used an earlier model version that relies on NDVI to estimate leaf area index (LAI), and focused on simulating the seasonal cycle of CO_2 fluxes using meteorological data for one year. The version 4.1.1 used in this study utilizes daily climate data, vegetation, plant functional type, soil and terrain conditions, and does not require satellite-NDVI data. Thus this version enables us to calculate the terrestrial carbon fluxes for a longer time period whenever daily meteorological data are available. The meteorological data required by Biome-BGC are preprocessed using MT-CLIM (Mountain Climate Simulator, Thornton and Running, 1999; Thornton et al., 2000), from the temperature and precipitation data provided by the 6-hourly NCEP (National Center for Environmental Prediction) reanalysis dataset (Kalnay et al., 1996). Biome-BGC estimates gross primary production (GPP) based on the models of Farquhar et al. (1980) and Leuning (1990) that employ estimates of leaf conductance, leaf nitrogen, intercellular CO_2 concentration, air temperature, incident solar radiation and LAI. CO_2 is released from carbon compartments through maintenance respiration (MR), growth respiration (GR) and heterotrophic respiration (HR) as prescribed algorithms that include controls by temperature and water. Thus, net primary production (NPP) is obtained as NPP = GPP−MR−GR, and NEP then is obtained as NEP = NPP−HR. Since we focused our study on the variations of NEP attributed to climate change, we ignored the CO_2 fertilization effect by keeping atmospheric CO_2 constant at 350 and 340 ppmv in simulating the seasonal cycle at a steady state and long-term trend for the period from 1961 to 1997, respectively. We also ignored nitrogen loading changes.

The input data for MT-CLIM (a preprocessor for climate data) and Biome-BGC are summarized in Tables 1 and 2 and Tables 3 and 4, respectively. MT-CLIM requires data for aspect, slope and horizon at each site as input information. It is difficult to provide accurate values of these parameters at each $1^\circ \times 1^\circ$ grid, and there are some uncertainties. Therefore, to check the sensitivity of MT-CLIM to the uncertainties of these geographical parameter values, we performed calculations using values ranging ±50% of aspect, ±180° of slope and 1°–10° of horizon from the standard case shown in Tables 1 and 2, at four selected sites: needle leaf forest in Siberia, grassland in North America (C3 grassland), grassland in Africa (C4 grassland) and evergreen forest in Amazon. Among the output values, vapor pressure deficit and shortwave

Table 2. *Parameters for MTCLIM (globally constant)*

Parameter	Value
Base annual precipitation isohyet	1.0 cm
Site east/west horizon	0.0°/0.0°
Maximum temperature lapse rate	-6.0°C km^{-1}
Minimum temperature lapse rate	-3.0°C km^{-1}

Table 1. *Input dataset for MTCLIM version 4.3*

Data	Reference	
Daily maximum/ minimum temperature	NCEP/NCAR reanalysis data, 2 m above ground Horizontal: T62, time step: 6 h	Kalnay et al. (1996)
Daily total precipitation	NCEP/NCAR reanalysis data, Horizontal: T62, time step: 6 h	Kalnay et al. (1996)
Elevation	FNOC elevation data	Cuming and Hawkins (1981)
Aspect	FNOC elevation data	Cuming and Hawkins (1981)
Slope	Surface slope data	Staub and Rosenzweig (1986)

Table 3. *Input dataset for Biome-BGC version 4.1.1*

Data	Description	Reference
Daily meteorological data	Daily maximum and minimum temperature data	Kalnay et al. (1996)
	Daily total precipitation	
	(*The following parameters are generated by MT-CLIM*)	see text
	Daylight average temperature	
	Daylight average partial pressure of water vapor	
	Daylight average short-wave radiant flux density	
Land cover type	Daylight Global potential vegetation map	Matthews (1983)
Soil texture	Sand/silt/clay percentage by volume	Webb et al. (1991)
	Depth : 30 cm (globally constant)	
Elevation	FNOC elevation data	Cuming and Hawkins (1981)
Short-wave albedo	Matthews seasonal albedo	Matthews (1983)

radiant flux density showed the most significant deviations from the standard run with the parameter values listed in Tables 3 and 4, but the overall deviations were less than 1% of annually averaged values. The results indicate that Biome-BGC is not significantly sensitive to the uncertainties in the values of the geographical parameters.

Before we started to calculate NEP variations over 37 yr, Biome-BGC was integrated for each $1^\circ \times 1^\circ$ grid point iteratively using the climate data for the period from 1961 to 1997 until the ecosystem at that point reached a steady state in which the annual NPP balanced the annual HR (Law et al., 2001; Thornton et al., 2002). To obtain CO_2 fluxes for model intercomparison of seasonal CO_2 simulation, the 1990 climate data was used, because the monthly NEP of CASA was calculated using the 1990 satellite-NDVI data as described later in section 2.1.3.

Table 4. *Parameters for Biome-BGC (globally constant)*

Parameter	Value
Atmospheric CO_2 concentration	350 ppmv for seasonal simulation
	340 ppmv for inter-annual simulation
Effective soil depth	1.0 m
Nitrogen deposition (atmospheric)	0.0001 kg m^{-2} yr^{-1}
Nitrogen fixation	0.0008 kg m^{-2} yr^{-1}
Industrial nitrogen deposition	0.0001 kg m^{-2} yr^{-1}

2.1.2. Sim-CYCLE. The Sim-CYCLE is an ecosystem model that is based on the dry-matter production theory (Monsi and Saeki, 1953) and was expanded for simulating the terrestrial carbon dynamics on a global scale (Ito and Oikawa, 2000). Using the monthly NCEP reanalysis data as input, Sim-CYCLE calculates monthly carbon fluxes between the atmosphere and the vegetation and soil/litter pools. Compared to Biome-BGC, Sim-CYCLE uses input data of lower temporal resolution; Biome-BGC calculates daily ecosystem cycles of carbon, nitrogen and water using daily climate data. In this study, the assessment of inter-annual variability among the ecosystem models and the observation was conducted using the time series of monthly NEP obtained from the model runs for the period 1961–1998. For the assessment of the seasonal CO_2 cycle, monthly NEP fluxes calculated for a year under averaged climatic conditions of 1961–1998 were used.

2.1.3. CASA. CASA relies on both satellite data and a mechanistic plant and soil carbon model to simulate a flow of carbon through terrestrial ecosystems. It applies a light-use efficiency to determine NPP at the global scale, using absorbed photosynthetically active radiation (APAR) from satellite data (Potter et al., 1993; Field et al., 1995). Carbon turnover is calculated mechanistically through a process-based plant and soil carbon cycling model. The monthly NEP fluxes we used for the seasonal model simulation were the same ones used in the TransCom-3 project (Gurney et al., 2002). The fluxes are calculated using NDVI of 1990 NOAA/NASA Pathfinder dataset and averaged temperature and precipitation over 1950–1980 (Randerson

et al., 1997), and are in equilibrium such that the annual flux at each point is zero.

2.2. Other CO_2 sources and sinks

Monthly net CO_2 fluxes between the atmosphere and the oceans were obtained from Takahashi et al. (2002). These net oceanic fluxes are based on about 2.5 million ΔpCO_2 measurements since 1960, and only non-El Niño conditions are selected to provide climatological monthly fields for a year. The ocean fluxes are seasonally changing, and the estimate of annual net global oceanic CO_2 uptake is about 2.2 GtC yr^{-1}. Since we focused only on the anomalies in terrestrial biospheric CO_2 flux in this study, the same monthly oceanic CO_2 fluxes without year-to-year change were used repeatedly over the computation period.

We used global fossil-fuel consumption data up to 1996 that were compiled by Marland et al. (1999), and the 1997 emission rate was assumed to be the same as in 1996. Brenkert (1998) reported the spatial distribution of fossil fuel usage on a $1^\circ \times 1^\circ$ grid for 1995, and the distribution was assumed not to change for the computation period. In order to quantify the seasonal cycle of fossil fuel emissions, Rotty (1987) investigated monthly emission rates of fossil fuels for 21 countries that consumed approximately 87% of the global total, mostly in the Northern Hemisphere. On average, the maximum appears in January and the minimum in August. This indicates that the heating usage in winter is the major contributor to the seasonal cycle of fossil-fuel emission in the Northern Hemisphere. Since other countries that are not included in Rotty (1987) are mostly in the tropical region with relatively small fossil fuel emissions characterized by very little seasonality, they are not expected to have a significant effect on the model results. Therefore we assumed no seasonality in fossil fuel emission in those countries.

The anthropogenic CO_2 flux due to land-use change, such as biomass burning and deforestation, was also included. Up to 1990, the annual emission rate and its geographical distribution compiled by Houghton and Hackler (2001) were used; in the model integration for years after 1990, the 1990 emission data were used. We did not include the CO_2 flux from biomass burning for seasonal cycle simulation because the seasonality of biomass burning is statistically uncertain, and it would produce a minimal effect mostly in the tropical region (Hao and Liu, 1994; Iacobellis et al., 1994; Randerson et al., 1997).

2.3. Atmospheric transport model

A three-dimensional atmospheric transport model (Maksyutov and Inoue, 2000) was used in the present study. The model has a horizontal resolution of $2.5^\circ \times 2.5^\circ$, 14 layers in the vertical dimension, and a numerical time step of about 15 min. The mass conservation in semi-Lagrangian advection is enforced by a mass fixer. The cumulus convection and planetary boundary layer (PBL) mixing are parameterized. Climatological PBL height at $2^\circ \times 2.5^\circ$ resolution is derived from the 3-hourly NASA GEOS-1 reanalysis data (Schubert et al., 1993). The model is driven by the analyzed wind field obtained from the European Center for Medium-Range Weather Forecasts (ECMWF, 1999). For this study, we used the ECMWF operational analyses for 1997. The transport model was run with the 1997 wind field repeatedly throughout the computation period. In other words, inter-annual variability in the CO_2 concentration due to atmospheric transport was ignored. Although this assumption appears to contradict the results obtained by Higuchi et al. (2002) and Dargaville et al. (2000), our investigation shows that the use of a non-interannually varying wind field introduces only about half of a ppmv bias in interannual variability of global atmospheric CO_2 in our study.

2.4. Atmospheric CO_2 observations

2.4.1. Seasonal cycle. For the observation against which the modeled atmospheric CO_2 seasonal cycles are to be compared, we used the background measurement data provided by NOAA/CMDL (National Oceanographic and Atmospheric Administration/Climate Monitoring and Diagnosis Laboratory, USA) (Conway et al., 1994), WMO/WDCGG (World Meteorological Organization/World Data Center for Greenhouse Gases) (WMO WDCGG, 2000) and Tohoku University (Nakazawa et al., 1993). Most of the NOAA/CMDL monitoring stations are located at coastal sites. Since atmospheric CO_2 signals at inland sites are strongly influenced by regional biospheric activities, the observation and modelling studies over continents are necessary to improve understanding of the terrestrial processes. As an example of continental observations, we used the station data at Monte Cimone, Italy ($44^\circ 11'$N, $10^\circ 42'$E) and at Mt. Waliguan, P. R. of China ($36^\circ 17'$N, $100^\circ 54'$E) (WMO WDCGG, 2000). Also, to examine model performance in simulating seasonal cycles of atmospheric CO_2 above the atmospheric boundary layer, we used the aircraft measurements of atmospheric CO_2 over Japan

Table 5. *Monitoring sites selected for this study to compare mean seasonal cycle*

Site code	Site	Country	Latitude	Longitude	Altitude
ALT[a,b]	Alert, North West Territories	Canada	87°27′N	62°31′W	210 m
BRW[a,b]	Pt. Barrow, Alaska	U.S.A.	71°19′N	156°36′W	11 m
SHM[a]	Shemya Island	U.S.A.	52°43′N	174°06′E	40 m
CMN[c]	Monte Cimone	Italy	44°11′N	10°42′E	2165 m
RYO[c]	Ryori	Japan	39°02′N	141°50′E	230 m
WLG[b,c]	Mt. Waliguan	P.R. China	36°17′N	100°54′E	3810 m
JP46[b,d]	Sendai–Fukuoka	Japan	33–37°N	130–140°E	4–6 km
MNM[c]	Minamitorishima	Japan	24°18′N	153°58′E	8 m
MLO[a,b]	Mauna Loa, Hawaii	U.S.A.	19°32′N	155°35′W	3397 m
KUM[a]	Cape Kumikahi, Hawaii	U.S.A.	19°31′N	154°49′W	3 m
SEY[a]	Seychelles (Mahe Island)	U.S.A.	4°40′S	55°10′E	3 m
SMO[a,b]	American Samoa	U.S.A.	14°15′S	170°34′W	30 m
CGO[a,b]	Cape Grim, Tasmania	Australia	40°41′S	144°41′E	94 m
SYO[a]	Syowa Station	Antarctica	69°00′S	39°35′E	11 m
SPO[a,b]	South Pole	Antarctica	89°59′S	24°48′W	2810 m

[a]NOAA/CMDL (Conway et al., 1994).
[b]Selected sites shown in Fig. 3.
[c]WMO/WDGCC (2000).
[d]Tohoku University (Nakazawa et al., 1993).

by Tohoku University (Nakazawa et al., 1993). A total of 15 ground and aircraft measurement locations used in this study for comparison with the model output are listed in Table 5, and their locations are shown in Fig. 1.

The time periods of observational data vary among sites. The shortest period is 6 yr at Mt. Waliguan; however, 6 yr would be long enough to derive a mean seasonal cycle. All the observational data were decomposed into seasonal and long-term components using a curve-fitting technique (Nakazawa et al., 1997a). For the present study, we used mean seasonal cycles, which are composed of the first two harmonics.

2.4.2. Inter-annual variations. As an indicator of global atmospheric CO_2 level, we used a combination of the observations at Mauna Loa, Hawaii (19°N) and the South Pole (90°S) (Keeling and Whorf, 2000). To obtain concentration anomalies caused by climate-related imbalance in CO_2 exchange between the atmosphere and the other carbon reservoirs, we first removed seasonal components from the observed CO_2 records by the same curve-fitting technique (Nakazawa et al., 1997a) employed for the seasonal cycle in section 2.4.1. From the resulting averaged deseasonalized global CO_2, we then subtracted a long-term trend obtained by smoothing with a Reinsch-type cubic spline having a cut-off period of 15 yr. The smoothed trend was regarded as a result of contributions by continuous anthropogenic CO_2 emission to the atmosphere, by biospheric response to constantly changing environmental conditions, such as increasing CO_2 concentration, and by oceanic CO_2 uptake due to increasing atmospheric CO_2 loading.

3. Methods

After being interpolated to monthly value fluxes on a $2.5^\circ \times 2.5^\circ$ grid, all the CO_2 sources from the surface are used as an input to the atmospheric transport model. For the seasonal simulation experiments, the atmospheric transport model was run with all the CO_2 fluxes, first for 2 yr as a spin-up, and then for 1 yr more for analysis. The annual total fossil-fuel emission for 1997 was used corresponding to the year 1997 transport. Each of NEP estimated at a steady state by the three TBMs was input in into the transport model. For the inter-annual simulations, the transport model was integrated first with the 1961 CO_2 fluxes for 2 yr and then for 37 yr more with the time-dependent monthly CO_2 fluxes.

3.1. Seasonal cycle

To compare the mean seasonal cycle of atmospheric CO_2 between the three simulation results and the observations at the monitoring sites listed in

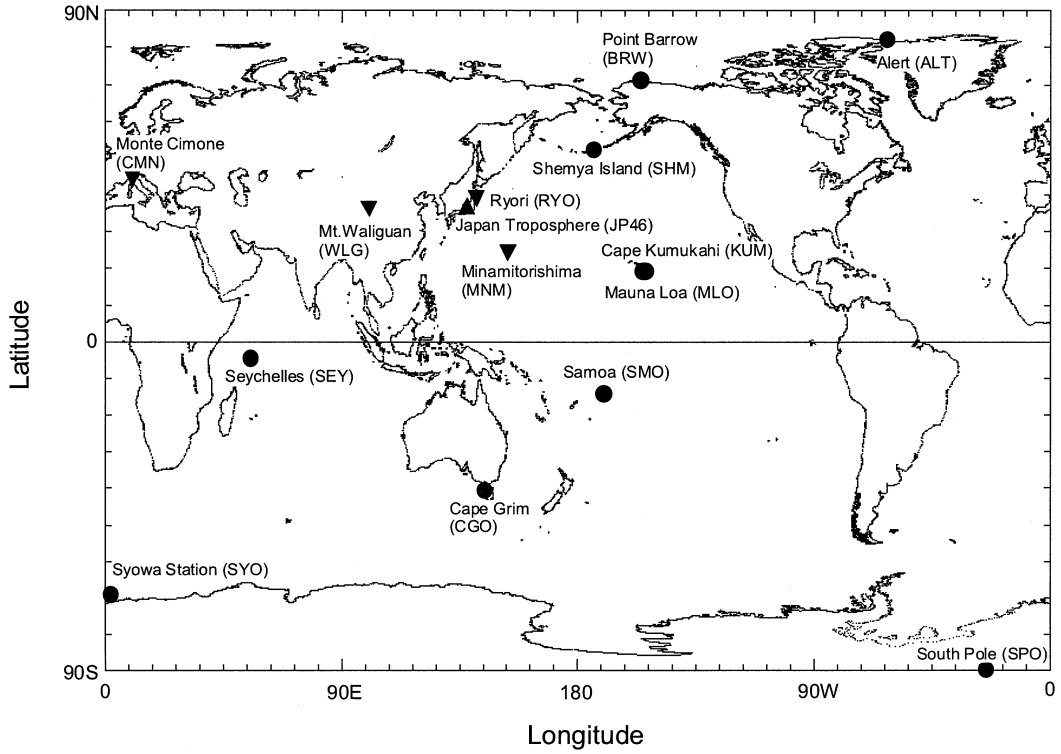

Fig. 1. Monitoring sites used for comparisons in this study. The site information is listed in Table 5. ●, NOAA/CMDL network stations; ▼, WMO/WDCGG; ▲, Tohoku University.

Table 5, seasonal components of the simulated atmospheric CO_2 concentrations were derived using the same curve-fitting procedure applied to the observational data. To evaluate how well Biome-BGC and the other ecosystem models simulated the observed seasonal signal of atmospheric CO_2 at each monitoring site k, we calculated the amplitude (A_k) and phase (P_k) parameters defined in the following way, similar to the footprint analysis by Randerson et al. (1997):

$$A_k = \frac{\sum_{m=1}^{12} |C_k(m)|}{\sum_{m=1}^{12} |C_{\mathrm{obs},k}(m)|} \tag{1}$$

where $C_{\mathrm{obs},k}(m)$ and $C_k(m)$ are the observed and calculated atmospheric CO_2, respectively, for each month ($m = 1, 2, \ldots, 12$) at each monitoring site k. For the phase variable, we have

$$P_k = \frac{\sum_{m=1}^{12} C_{\mathrm{obs},k}(m) \times C_k(m)}{\sqrt{\sum_{m=1}^{12} [C_{\mathrm{obs},k}(m)]^2 \times \sum_{m=1}^{12} [C_k(m)]^2}}. \tag{2}$$

The phase parameter P_k varies between 1 and –1, as the calculated seasonal cycle changes from completely in phase to completely out of phase with the observation.

3.2. Inter-annual variations

NEP is affected by changes in climate parameters such as air temperature and precipitation. This results in monthly deviations in NEP from a steady state. The deviations are small relative to monthly gross CO_2 fluxes between the biosphere and the atmosphere, but large enough to affect global CO_2 trends.

Firstly, we investigated the global anomaly of modeled NEP. The NEP anomaly [$Anom(t)_m$] is defined as the difference between global NEP in a given month

of a given year and the multi-year averaged monthly NEP over the entire period:

$$Anom(t)_m = NEP(t)_m - NEP_{\mathrm{AVE},m} \quad (3)$$

where m denotes the mth month of a year, $NEP(t)_m$ is the global NEP at time of t, and $NEP_{\mathrm{AVE},m}$ is the multi-year average of NEP of the mth month over the period from 1961 to 1997.

Secondly, global CO_2 concentration anomalies in the model simulations were obtained by the same curve-fitting technique mentioned in section 2.4.2 applied to the simulated atmospheric CO_2 at Mauna Loa and the South Pole individually, and then averaged for comparison with the observed values. The same curve-fitting technique was applied because the simulated atmospheric CO_2 also contained both seasonal and inter-annual variations, as well as long-term trends. With the model results of Biome-BGC and Sim-CYCLE, linear correlations between both simulated and observed values were obtained for model inter-comparison.

4. Results and discussions

4.1. Net ecosystem production predicted by TBMs

To obtain a comparative overview of the net seasonal CO_2 fluxes between the atmosphere and the biosphere produced by Biome-BGC, the seasonal cycle of zonally averaged NEP by Biome-BGC is plotted in Fig. 2, along with those obtained by Sim-CYCLE and CASA.

In Fig. 2, all the model estimates show that the middle–high northern latitudes (north of 30°N) act as strong CO_2 sink from May to August, and as a source from October to March. However, to the south of the equator, regions in middle southern latitudes (30°–60°S) act as a CO_2 source from September to February. As seen in Fig. 2, all the models have some similarities, but the timing, magnitude and regions of CO_2 source and sink differ to some degree, depending on the differences in approach taken for calculating CO_2 fluxes, ecosystem types and meteorological data.

Overall, the seasonal pattern of NEP produced by Biome-BGC is similar to the one produced by CASA. Both of them have positive peaks from June to July over northern middle and high latitudes, but the source strength estimated by Biome-BGC is about half of that simulated by CASA, and the positive NEP appears earlier and persists longer by about 2 months than CASA. This longer positive duration indicates that Biome-BGC produces a longer growing season.

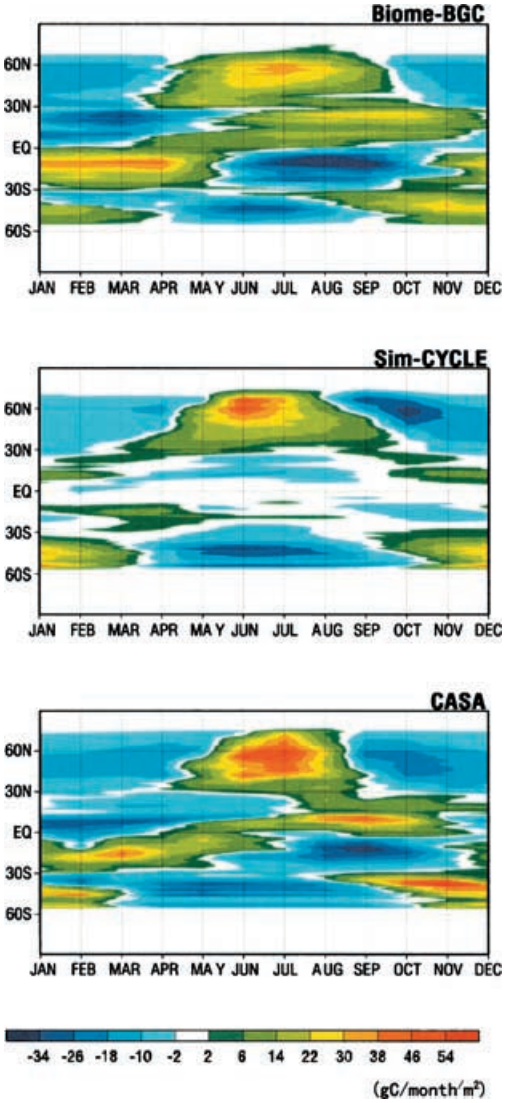

Fig. 2. Seasonal cycles of zonally averaged net ecosystem production (NEP) for each of TBMs. Units are (g C month $^{-1}$m^{-2}) of land area. Positive values mean net CO_2 uptake by the ecosystems from the atmosphere, while negative mean net CO_2 release from the ecosystems to the atmosphere. It is noted that the zonal averages are plotted, as interpolated along January to December from monthly net fluxes, on the assumption that each monthly flux is the value on the middle day of each month.

Both Biome-BGC and CASA show approximately opposite seasonal patterns in the northern and southern lower latitudes. In regions north of 50°N, Sim-CYCLE produces a strong net accumulation from the end of

May to early June, and a strong CO_2 release from September to November. The positive NEP duration from April to September estimated by Sim-CYCLE is similar to the Biome-BGC estimate, but an early strong accumulation peak and intensive CO_2 release just after the growing season are characteristic of the Sim-CYCLE model and not apparent in Biome-BGC. Another distinctive difference of Sim-CYCLE from the other TBMs is that almost no seasonality in biospheric activities in the tropical region is produced.

The comparison of the flux seasonality suggests that both process-based, climate-only driven models like Biome-BGC and Sim-CYCLE have a longer period of biogenic activity in mid to high latitudes in the Northern Hemisphere, as compared to the CASA model, which is constrained by the NDVI greenness.

4.2. *Comparisons of mean seasonal cycles to the observations*

Values of A_k and P_k calculated using eqs. (1) and (2) for each of the terrestrial ecosystem models at various monitoring sites are summarized in Tables 6 and 7, respectively.

As seen in Tables 6 and 7, Biome-BGC reproduced well the observed phases of the seasonal cycles at all sites. The averaged value of P_k over all the northern sites considered in this study is 0.95, close to that of CASA, which showed the best performance in the Northern Hemisphere in terms of phase. On the other hand, the simulated amplitudes by Biome-BGC in the Northern Hemisphere were small compared to the observations and to the other models simulations. These smaller amplitudes mainly result from the underestimation of NEP strengths in middle and high northern latitudes, as is shown in Fig. 2.

Table 6. *Comparisons of mean seasonal amplitude between modeled estimate and observation*

Site	Biome-BGC	Sim-CYCLE	CASA
ALT	0.73	0.97	0.84
BRW	0.82	1.23	0.96
SHM	0.65	1.23	0.73
CMN	0.65	0.52	0.57
RYO	0.94	0.62	1.16
JP46	0.83	0.65	0.95
MNM	0.92	0.79	0.89
WLG	0.91	1.33	2.10
MLO	0.73	0.62	0.85
KUM	0.73	1.10	0.85
SEY	0.69	1.11	1.03
SMO	1.43	3.78	2.31
CGO	1.52	2.39	1.12
SYO	1.57	1.48	1.76
SPO	1.57	1.49	1.76
Average			
Northern Hemisphere	0.79	0.91	0.99
Southern Hemisphere	1.35	2.05	1.60

Table 7. *Comparisons mean seasonal phase between modeled estimate and observation*

Site	Biome-BGC	Sim-CYCLE	CASA
ALT	0.97	0.77	0.98
BRW	0.94	0.75	0.95
SHM	0.90	0.78	0.99
CMN	0.93	0.98	0.97
RYO	0.90	0.86	0.98
JP46	0.98	0.99	0.98
MNM	0.94	0.91	0.99
WLG	0.98	0.32	0.94
MLO	0.96	0.91	0.99
KUM	0.96	0.61	0.98
SEY	0.95	0.93	0.97
SMO	0.87	-0.14	0.94
CGO	0.96	0.70	0.52
SYO	0.99	0.80	0.90
SPO	0.99	0.83	0.92
Average			
Northern Hemisphere	0.95	0.79	0.98
Southern Hemisphere	0.95	0.63	0.85

In order to assess the ability of Biome-BGC in simulating the observed latitudinal variation of the seasonal cycle, we chose eight monitoring sites as representatives of the low, middle and high latitudes of each hemisphere. For each of the selected sites, Fig. 3 shows the simulated mean seasonal cycle by each of the ecosystem models, as well as the observation from the site for comparison.

At Alert (ALT: 87°27′N, 62°31′W) and Pt. Barrow (BRW: 71°19′N, 156°36′W) in the northern higher latitudes, the seasonal maximum simulated with Biome-BGC appears one month earlier than the observation (Figs. 3a and 3b). This tendency is also seen over Japan (JP46: 33–37°N, 130–140°E, 4–6 km) in middle latitudes (Fig. 3d) and at Mauna Loa, Hawaii (MLO: 19°32′N, 155°35′W) in low latitudes (Fig. 3e). The seasonal minima simulated with Biome-BGC appear

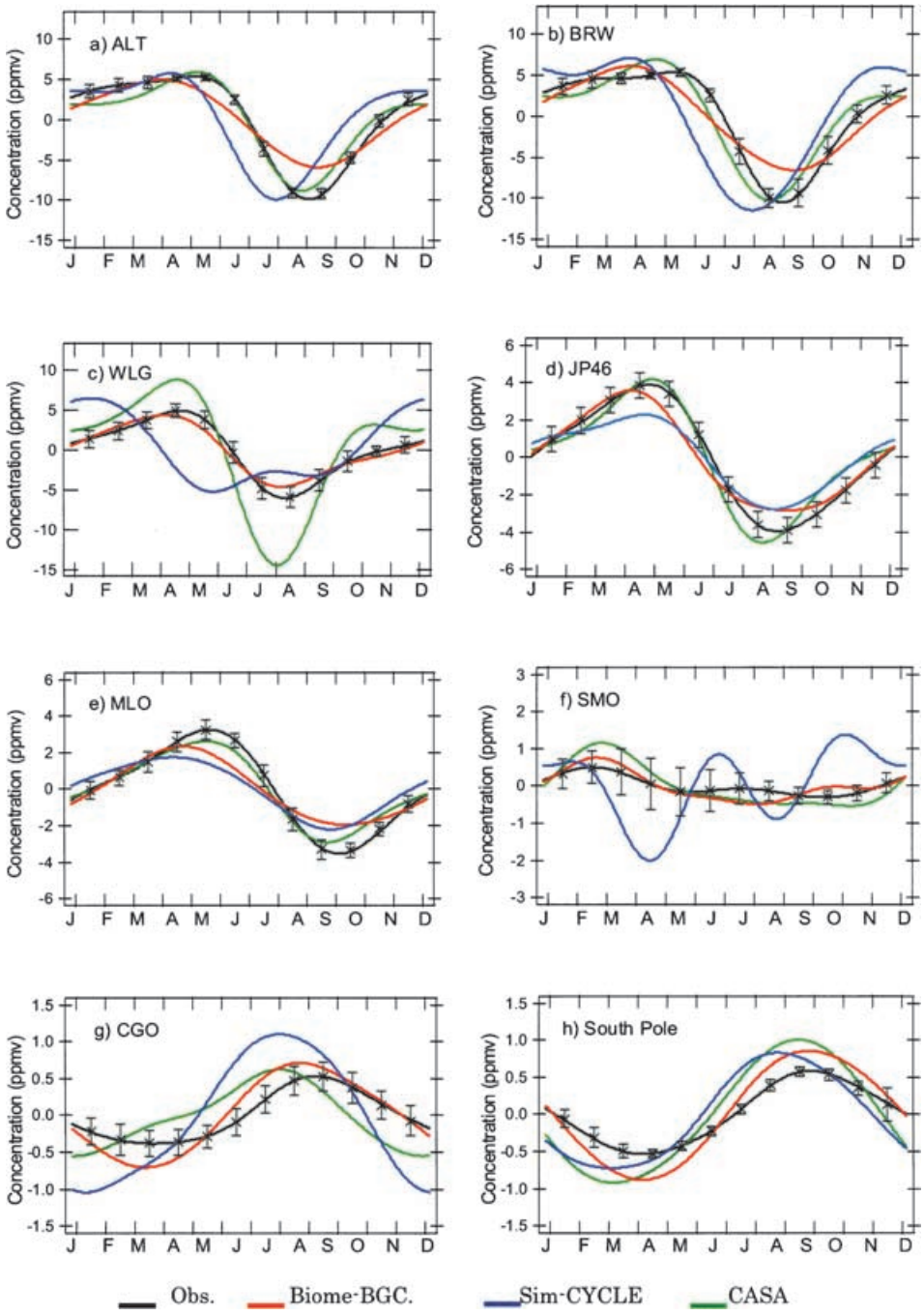

Fig. 3. Comparison of the observed seasonal cycle of atmospheric CO_2 concentration at eight selected monitoring stations with the simulated seasonal cycle with the monthly estimates of NEP by three TBMs: Biome-BGC, Sim-CYCLE and CASA: (a) ALT (Alert), (b) BRW (Pt. Barrow), (c) JP46 (Japan troposphere, at altitude of 4–6 km), (d) WLG (Mt. Waliguan), (e) MLO (Mauna Loa), (f) SMO (American Samoa), (g) CGO (Cape Grim), (h) SPO (South Pole). Error bars are standard deviations.

slightly later than the observation at ALT and BRW, but the timing at JP46 and MLO are reproduced well with Biome-BGC; however, the CO_2 recovery after the minimum is slow, compared with the other models and the observation. In the Northern Hemisphere, the seasonal cycles of atmospheric CO_2 are controlled mostly by the CO_2 exchange with the terrestrial biosphere (e.g., Fung et al., 1983; Keeling et al., 1989; Nakazawa et al., 1997b). The early drawdown of CO_2 simulated with Biome-BGC results from the early start of the growing season, as mentioned already with regard to NEP. The slow CO_2 recovery by Biome-BGC indicates that the moderate soil decomposition takes place throughout the winter season as illustrated in Fig. 2a, in contrast to a stronger decomposition in autumn by Sim-CYCLE.

Mt. Waliguan (WLG: 36°17′N, 100°54′E) is located at the north-east edge of the Tibetan Plateau. The observed seasonal phase at WLG is similar to JP46, which is located almost in the same latitude band, but higher in altitude by 1–2 km. Biome-BGC shows the best performance at WLG ($P_k = 0.98, A_k = 0.91$); however, matching the seasonal amplitudes is dependent on the validity of the transport model, which may overestimate vertical mixing over mountains. The timing of the seasonal minimum and maximum simulated by CASA is slightly delayed. Sim-CYCLE shows the least agreement with the observed phase at WLG. Both CASA and Sim-CYCLE produce larger amplitudes than the observation. WGL is surrounded by semi-arid grassland and desert, and there is no large local CO_2 source. The observed CO_2 concentration therefore likely reflects the ′background′ characteristics over Northern China. Compared to Biome-BGC, the other TBMs suggest stronger seasonal biospheric CO_2 fluxes over the mountainous area and inland China.

All of the modeled estimates show relatively good agreement with the observed phase in 4–6 km of altitude over Japan (Fig. 3d). The estimated phase delays in the troposphere are less than half of a month. It is notable that Sim-CYCLE underestimates the seasonal amplitude in the free atmosphere over Japan, as well as at ground stations, Ryori, Japan (RYO: 39°02′N, 141°50′E, 230 m) and Minamitorishima, Japan (MNM: 24°18′N, 153°58′E, 8 m) (Table 6). However, Sim-CYCLE approximately matches the amplitudes in the higher latitudes (ALT, BRW). Since the biospheric signal over Asia has a significant influence on the seasonal cycle over Japan, the smaller amplitude simulated there with Sim-CYCLE would indicate a weaker seasonality of CO_2 fluxes estimated over China and other parts of temperate Asia.

In the tropics, the contribution through atmospheric transport to the observed seasonal cycle by the fossil fuel emission in the Northern Hemisphere is comparable to the contributions from the local oceanic and bisopheric sources. At American Samoa (SMO: 14°15′S, 170°34′W), all the TBMs overestimate the seasonal amplitude, but Biome-BGC and CASA reproduce the phase of the observed seasonal cycle relatively well. The simulation with Sim-CYCLE does not capture the phase of the seasonal cycle, and the predicted amplitude is about twice as large as Biome-BGC and CASA. As long as the seasonality of the estimated NEP by Sim-CYCLE in the tropical regions is weak, the atmospheric seasonal cycle in the tropics is determined largely by the CO_2 signals from higher-latitude regions in the Northern Hemisphere through seasonally changing atmospheric transport.

At Cape Grim (CGO: 40°41′S, 144°41′E) and the South Pole (SPO: 89°59′S, 24°48′W), Biome-BGC shows the best agreement with the observed phase. However, it overestimates the seasonal amplitudes at these locations, like the other TBMs do. As the biospheric flux diminishes poleward in the Southern Hemisphere, contributions from the oceanic CO_2 exchange and the atmospheric transport become more significant. The results (not shown) suggest that the oceanic CO_2 signal on the seasonal cycle has a similar phase and comparable amplitude to the biospheric signal, thus enhancing the simulated seasonal amplitude. Therefore, the discrepancy in the seasonal cycle between the modeled estimate and the observation could be due to an improper estimate of oceanic CO_2 seasonality in the southern oceans. However, there is still a great deal of uncertainty in the estimation of oceanic fluxes, mainly due to limited field measurements. Another possible factor is an inaccurate atmospheric transport of CO_2 from the Northern Hemisphere.

Another issue in matching the seasonal cycle at CGO is that of ′background′ selection of data (Law, 1996; Ramonet and Monfray, 1996). Law (1996) showed that moving the CGO model grid point offshore can improve the data and model comparison in both phase and amplitude. In the present study, the nearest model grid point to CGO located off the coast of Tasmania (41°15′S, 143°45′E) was used. Sampling at points to the west and to the southwest of the CGO model grid point reduced the short-term variability but

led to only a little change in the amplitude of the seasonal cycle.

To summarize the overall performances of the three TBMs:

(1) Biome-BGC agrees well with the observed phases at all the selected sites over the globe. Biome-BGC tends to underestimate the amplitude of seasonal signals in the Northern Hemisphere, while it overestimates it in the Southern Hemisphere.

(2) CASA shows a good overall performance, especially in the Northern Hemisphere.

(3) Sim-CYCLE reproduces the observed amplitude in the higher northern latitudes, but its seasonal maximum and minimum are likely to appear earlier than the observed values by one month.

All the model simulations with respective TBMs show poor performance to some extent in the Southern Hemisphere where the seasonality of biospheric flux is much less pronounced than in the Northern Hemisphere. To explain the discrepancy between the model simulations and the observations, it is necessary to examine the uncertainty associated with the exchange of oceanic CO_2 with the atmosphere and to quantify the influence of the atmospheric transport.

Using the previous version of Biome-BGC, Hunt et al. (1996) demonstrated larger NEP and better agreement with the observation especially in the Northern Hemisphere. One of the possible causes in the difference between their results and ours could be in the way the LAI, which directly controls the canopy processes, is treated in the two versions of the model. The previous version used LAI estimated from the annual maximum NDVI for each grid to minimize the problems such as atmospheric conditions (Nemani and Running, 1996). On the other hand, the present version predicts LAI on a daily time step using environmental parameters, and the annual maximum LAI, on average, is underestimated in comparison with the previous version. Although the satellite-retrieved LAI depends on an empirical formulation of the NDVI–LAI relationship (e.g., Hunt et al., 1996; Myneni et al., 1997), it could be helpful to validate the Biome-BGC-produced LAI by comparing it with the satellite-retrieved LAI.

4.3. Interannual variability in net ecosystem production

The anomalies in global annually averaged NEP simulated by Biome-BGC and Sim-CYCLE are shown in Fig. 4, along with El Niño periods. Except for the period from 1991 to 1993, the calculated NEP shows positive anomalies during the El Niño events, during which net anomalous CO_2 is released from the terrestrial biosphere.

NEP is defined as net primary production (NPP) minus heterotrophic respiration (HR). The NEP anomaly calculated by Biome-BGC shows a much closer correlation with NPP ($R = 0.803$) than with HR ($R = 0.048$). This indicates that a change in photosynthetic

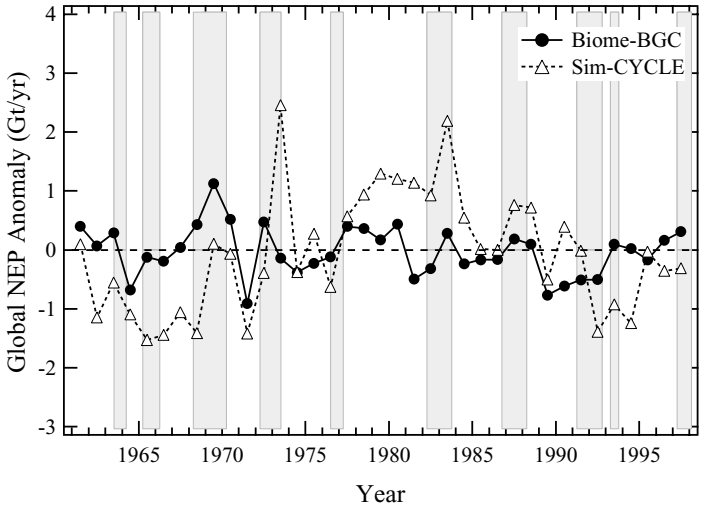

Fig. 4. Calculated global NEP anomalies. Shaded areas indicate El Niño events as identified by JMA SST index.

activity caused by climate change is a significant factor in the NEP anomaly. However, the simulated negative NEP anomaly over the period from 1991 to 1993 is attributable mainly to HR decrease. During that period, the effect of a relatively weak El Niño was masked by a strong air temperature decrease caused by the Mt. Pinatubo eruption in 1991 (Hansen, et al., 1992). This decrease in temperature lowered the overall soil respiration, allowing net uptake of CO_2 by the land biosphere. The NEP anomalies by Biome-BGC show a similar phase to those by Sim-CYCLE, especially after 1975. On the other hand, Biome-BGC has a smaller variability of ± 1 Gt C yr^{-1}, as compared to Sim-CYCLE with ± 2 Gt C yr^{-1}.

4.4. *Comparison of global anomalis in atmospheric CO_2 concentration*

Figures 5a and 5b show the simulated globally averaged CO_2 concentration anomalies, along with the

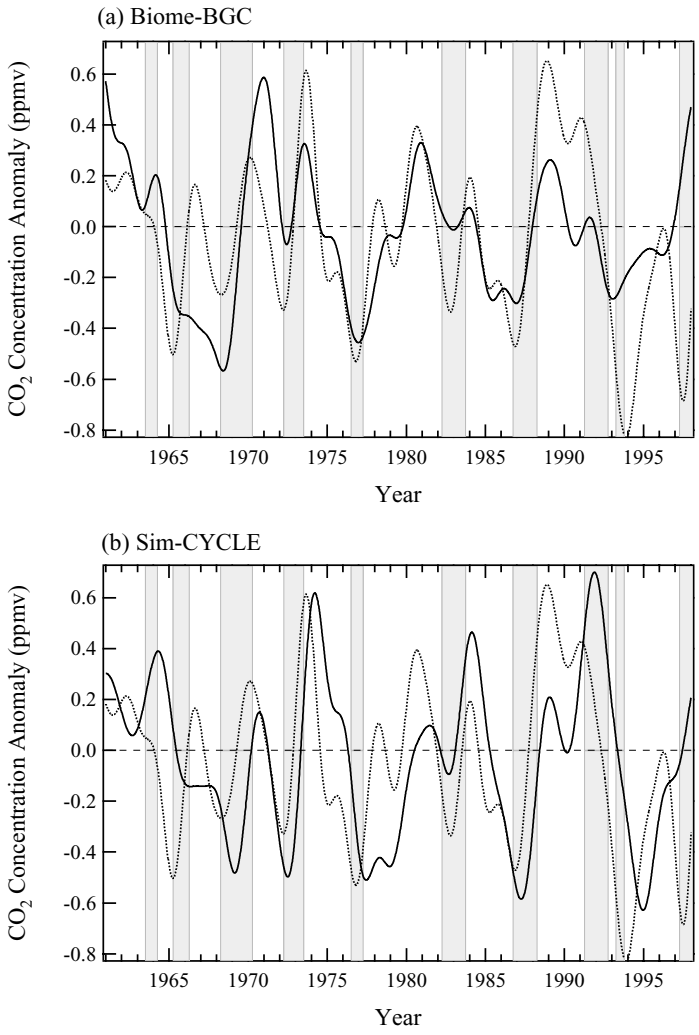

Fig. 5. Global anomaly in CO_2 concentration. Solid lines are the calculated anomalies with NEP by (a) Biome-BGC and (b) Sim-CYCLE. Dotted lines are anomalies obtained from the observations at Mauna Loa and the South Pole. Shaded areas indicate El Niño events.

observation (obtained by averaging data from Mauna Loa and the South Pole). El Niño events are also indicated. Except for the El Niño event in the early 1990s, it is obvious from Fig. 5a that the observed CO_2 increased either during the onset year of, or soon after each El Niño event. The simulated anomaly by Biome-BGC matches the phase of the observed anomaly, but the modeled amplitude of the inter-annual variation is smaller than the observed one (Fig. 5a). This comparison result suggests that a significant part of the inter-annual variability in the global carbon cycle can be attributed to an imbalance of the CO_2 exchange between the terrestrial biosphere and the atmosphere, as the oceanic inter-annual variability was not taken into account in this study. Our result therefore agrees with those of the most recent studies (e.g. Bousquet et al., 2000).

During an El Niño event, the upwelling of CO_2-rich deep water is suppressed in the equatorial Eastern Pacific, resulting in reduced oceanic CO_2 fluxes to the atmosphere (Feely et al., 1999). An El Niño event is also associated with temperature and precipitation anomalies worldwide. Increased temperature and reduced rainfall over land cause a reduction of photosynthesis and an increase in respiration and occurrences of wild fires (e.g., Keeling et al., 1995). Consistent with the above concept, Rayner et al. (1999) analyzed the correlation of tropical CO_2 sources with El Niño-Southern Oscillation (ENSO) events for the period 1980–1995 and found some indication of initial negative CO_2 anomaly response to the oceanic change due to ENSO, followed by anomalous positive CO_2 response to the subsequent terrestrial biospheric change in the tropical region. Therefore, had we included the effect of the oceanic CO_2 flux change in this study, it would have enhanced the magnitude of the negative CO_2 anomaly at the onset of an ENSO event, but it might have had less influence on the phasing of the simulated CO_2 anomalies.

As for the Pinatubo anomaly, when significant slowdown of the atmospheric CO_2 increase was observed globally, many studies have shown an increase in net biospheric uptake, as well as in oceanic uptake (e.g., Francey et al., 1995; Keeling et al., 1995). The model simulation with Biome-BGC reproduced a negative CO_2 anomaly due to the net biospheric uptake during the period 1991–1993, but did not capture the magnitude of the dip. One could suggest that the discrepancy is caused by the neglect of oceanic CO_2 flux change. Feely et al. (1999) estimated that the decrease of the release of oceanic CO_2 flux to the atmosphere over the equatorial pacific region during the 1991–1994 El Niño period amounted to 0.8–1.2 Gt C. This estimated reduction is comparable to the difference between the simulated and observed data in our study.

The simulations performed with predicted biospheric CO_2 fluxes by Sim-CYCLE showed larger magnitudes of inter-annual variability in atmospheric CO_2, which is closer to the observed range, but with more visible phase mismatches at a number of extreme anomalous events (Fig. 5b). The linear correlation coefficient between the Sim-CYCLE modeled anomaly and the observed anomaly was 0.37, while that with Biome-BGC was 0.67. These results show that Biome-BGC has a better performance in reproducing the phase of the long-term variability than Sim-CYCLE.

Similar differences between the two models are seen in the simulations of the atmospheric CO_2 seasonal cycle. Generally, Biome-BGC reproduced well the timing of the seasonal cycle, but its predicted seasonal amplitude was relatively small in the northern high latitudes, compared to the observation and to Sim-CYCLE and CASA. These weaker atmospheric CO_2 signals predicted by Biome-BGC may indicate a need for enhancement in the sensitivity of Biome-BGC modeled fluxes to seasonal and inter-annual changes in temperature and precipitation.

4.5. Effects of uncertainties in Biome-BGC model assumptions

During the simulation period from 1961 to 1997, we assumed a constant atmospheric CO_2 level at 340 ppmv, to ignore the CO_2 fertilization effect on the inter-annual simulation. To test the effect of a changing CO_2 concentration, we performed model experiments with several different CO_2 concentration levels, ranging from 290 to 360 ppmv. The result is that the deviation of the global NEP caused by prescribing different levels of atmospheric CO_2 is only less than 10% from the standard case and the effect on the anomalous NEP is a few percent in the amplitude. When the nitrogen deposition from the atmosphere and fixation were changed by $\pm 10\%$, the change in the global NEP was less than 1%. These CO_2 and nitrogen fertilization effects on NEP could gradually increase in a long term. Therefore, these effects might have an impact on the seasonal and inter-annual variations of NEP, but with low sensitivity.

5. Summary

In order to investigate the seasonal and inter-annual variability of the global atmospheric CO_2 concentration during the period 1961–1997, we drove an atmospheric transport model with CO_2 fluxes calculated by a terrestrial biosphere model Biome-BGC. The simulated CO_2 concentration anomalies matched the phase of the observed inter-annual CO_2 variability, even without taking into account the inter-annual variability of the atmospheric transport and oceanic flux. The result therefore suggests that a significant part of the inter-annual variability in the global carbon cycle can be attributed to changes in the terrestrial biosphere.

For model validation, we examined the simulated seasonal CO_2 signals by comparing them to the observations. Biome-BGC reproduced well the timing of the seasonal cycle of atmospheric CO_2, but underestimated the amplitude in the Northern Hemisphere, where the biospheric CO_2 signal is dominant. A similarity in model-to-model difference was found in terms of sensitivities to climate variations, both in the short term (seasonal cycle amplitude) and long term (amplitude of the inter-annual variations). Biome-BGC better reproduced phases of both seasonal and inter-annual variability than Sim-CYCLE, while it showed weaker amplitudes of inter-annual variability and seasonal cycles of atmospheric CO_2, except in the northern middle latitudes. This may indicate a need for further improvement of Biome-BGC model sensitivity to climate parameters.

The present analysis of inter-annual variability focused only on a global scale. The next step will include examination at a regional scale to identify areas that make significant contributions to the inter-annual variability of atmospheric CO_2.

6. Acknowledgments

We are grateful to A. Ito, who kindly provided Sim-CYCLE model output. The Biome-BGC model was provided by the Numerical Terradynamic Simulation Group (NTSG) at the University of Montana. We also thank S. Running, D. Dye, G. Churkina and K. Higuchi for their comments on our model study. We thank the anonymous reviewers for constructive comments on our original submission. The reviewers′ valuable suggestions have contributed to a significant improvement in the paper.

REFERENCES

Bousquet, P., Peylin, P., Ciais, P., Le Quere, C., Friedlingstein, P. and Tans, P. P. 2000, Regional changes in carbon dioxide fluxes of land and oceans since 1980. *Science* **290**, 1342–1346.

Brenkert, A. L. 1998. Carbon dioxide emission estimates from fossil-fuel Burning, hydraulic cement production, and gas flaring for 1995 on a one degree grid cell basis. NDP-058A, CDIAC, ORNL, Oak Ridge, Tenn., USA.

Conway, T. J., Tans, P. P., Waterman, L. S., Thoning, K. W., Kitzis, D. R., Masarie, K. A. and Ni, Z. 1994. Evidence for interannual variability of the carbon cycle from the National Oceanic and Atmospheric Administration/Climate Monitoring and Diagnostics Laboratory Global Air Sampling Network. *J. Geophys. Res.* **99**, 22831–22855.

Cuming, M. J. and Hawkins, B. A. 1981. TERDAT: The FNOC system for terrain data extraction and processing. In: *Technical report MII Project M-254*, Fleet Numerical Oceanography Center, Monterey, Calif., USA.

Dargaville, R., Law, R. M. and Pribac, F. 2000. Implications of interannual variability in atmospheric circulation on modeled CO_2 concentrations and source estimates. *Global Biogeochem. Cycles* **14**, 931–943.

ECMWF. 1999. ECMWF/WCRP Level III-A Global Atmospheric Data Archive, ECMWF, http://www.ecmwf.int.

Farquhar, G. D., Van Caemmerer, S. and Berry, J. A. 1980. A biochemical model of photosynthetic CO_2 assimilation in leaves of C3 species. *Planta* **149**, 78–90.

Feely, R. A., Wanninkhof, R., Takahashi, T. and Tans, P. 1999. Influence of El Niño on the equatorial Pacific contribution to atmospheric CO_2 accumulation. *Nature* **398**, 597–601.

Field, C. B., Randerson, J. T. and Malmstron, C. M. 1995. Global net primary production: combining ecology and remote sensing. *Remote Sens. Environ.* **51**, 74–88.

Francey, R. J., Tans, P. P., Allison, C. E., Enting, I. G., White, J. W. and Trolier, M. 1995. Changes in oceanic and terrestrial carbon uptake since 1982. *Nature* **373**, 326–330.

Fung, I., Tucker, C. J. and Prentice, K. C. 1987. Application of advanced very high resolution radiometer vegetation index to study atmosphere–biosphere exchange of CO_2. *J. Geophys. Res.* **92**, 2999–3015.

Gurney, K. R., Law, R. R., Denning, A. S., Rayner, P. J., Baker, D., Bousquet, P., Bruhwiler, L., Chen, Y.-H., Ciais, P., Fan, S., Fung, I., Gloor, M., Heimann, M., Higuchi, K., John, J., Maki, T., Maksyutov, S., Masarie, K., Peylin, P., Prather, M., Pak, B. C., Randerson, J., Sarmiento, J., Taguchi, S., Takahashi, T. and Yuen, C.-W. 2002. Towards robust regional estimates of CO_2 sources and sinks using atmospheric transport models. *Nature* **415**, 626–630.

Hansen, J., Lacis, A., Ruedy, R. and Sato, M. 1992. Potential climate impact of Mount Pinatubo eruption. *Geophys. Res. Lett.* **19**, 215–218.

Hao, W. M. and Liu, M.-H. 1994. Spatial and temporal distribution of tropical biomass burning. *Global Biogeochem. Cycles* **8**, 495–503.

Heimann, M., Esser, G., Haxeltine, A., Kaduk, J., Kicklighter, D. W., Knorr, W., Kohlmaier, G. H., McGuire, A. D., Melillo, J., Moore, B., Otto, R. D., Prentice, I. C., Sauf, W., Schloss, A., Sitch, S., Wittenberg, U. and Wurth, G. 1998. Evaluation of terrestrial carbon cycle models through simulations of the seasonal cycle of atmospheric CO_2: First results of a model intercomparison study. *Global Biogeochem. Cycles* **12**, 1–24.

Higuchi, K., Murayama, S. and Taguchi, S. 2002. Quasi-decadal variation of the atmospheric CO_2 seasonal cycle due to atmospheric circulation changes: 1979–1998. *Geophys. Res. Lett*. **29**, 10.1029, 2001GL013751.

Houghton, R. A. and Hackler, J. L. 2001. Carbon flux to the atmosphere from land-use changes: 1850 to 1990. ORNL/CDIAC-131, NDP-050/R1, CDIAC, ORNL, Oak Ridge, Tenn., USA.

Hunt, Jr., E. R., Piper, S. C., Nemani, R., Keeling, C. D., Otto, R. D. and Running, S. W. 1996. Global net carbon exchange and inter-annual atmospheric CO_2 concentrations predicted by an ecosystem process model and three-dimensional atmospheric transport model. *Global Biogeochem. Cycles* **10**, 431–456.

Iacobellis, S. F., Frouin, R., Razafimpanilo, H., Somerville, R. C. J. and Piper, S. C. 1994. North African savanna fires and atmospheric carbon dioxide. *J. Geophys. Res*. **99**, 8321–8334.

Ito, A. and Oikawa, T. 2000. A model analysis of the relationship between climate perturbations and carbon budget anomalies in global terrestrial ecosystems: 1970 to 1997. *Climate Res.* **15**, 161–183.

Kalnay, E., Kanamitsu, M., Kistler, R., Collins, W., Deaven, D., Gandin, L., Iredell, M., Saha, S., White, G., Woollen, J., Zhu, Y., Chelliah, M., Ebisuzaki, W., Higgins, W., Janowiak, J., Mo, K. C., Ropelewski, C., Wang, J., Leetmaa, A., Reynolds, R., Jenne, R. and Joseph, D. 1996. The NCEP/NCAR 40-year reanalysis project. *Bull. Am. Meteorol. Soc.* **77**, 437–471.

Keeling, C. D. and Whorf, T. P. 2000. Atmospheric CO_2 records from sites in the SIO air sampling network. In: *Trends: a compendium of data on global change*. CDIAC, ORNL, Oak Ridge, Tenn., USA.

Keeling, C. D., Bacastow, R. B., Carter, A. F., Piper, S. C., Whorf, T. P., Heimann, M., Mook, W. G. and Roeloffzen, H. 1989. A three-dimensional model of atmospheric CO_2 transport based on observed winds: 1. Analysis of observed data. In: *Aspects of climate variability in the Pacific and western America* (ed. D. H. Peterson). *Geophys. Monogr.* **55**, 165–236, AGU, Washington DC, USA.

Keeling, C. D., Whorf, T. P., Wahlen, M. and Van der Plicht, J. 1995. Interannual extremes in the rate of rise of atmospheric carbon dioxide since 1980. *Nature* **375**, 666–670.

Law, B. E., Thornton, P. E., Irvine, J., Anthoni, P. M. and Van Tuyl, S. 2001. Carbon storage and fluxes in Ponderosa pine forests at different developmental stages. *Global Change Biol.* **7**, 755–777.

Law, R. 1996. The selection of model-generated CO_2 data: a case study with seasonal biospheric source. *Tellus* **48B**, 474–486.

Leuning, R. 1990. Modeling stomatal behavior and photosynthesis of *Eucalyptus grandis*. *Aust. J. Plant Physiol.* **17**, 159–175.

Marland, G., Andres, R. J., Boden, T. A., Johnston, C. A. and Brenkert, A. L. 1999. Global, Regional, and National CO_2 Emission Estimates from Fossil Fuel Burning, Cement Production, and Gas Flaring: 1751–1996 (revised March 1999). NDP-030, CDIAC, ORNL, Oak Ridge, Tenn., USA.

Maksyutov, S. and Inoue, G. 2000. Vertical profiles of radon and CO_2 simulated by the global atmospheric transport model. In: *CGER Supercomputer activity report*, I039–2000, **7**, 39–41, CGER NIES, Tsukuba, Japan.

Matthews, E. 1983. Global vegetation and land use: new high-resolution data bases for climate studies. *J. Clim. Appl. Meteorol*. **22**, 474–487.

McGuire, A. D., Sitch, S., Clein, J. S., Dargaville, R., Esser, G., Foley, J., Heimann, M., Joos, F., Kaplan, J., Kicklighter, D. W., Meier, R. A., Melillo, J. M., Moore III, B., Prentice, I. C., Ramankutty, N., Reichenau, T., Schloss, A., Tian, H., Williams, L. J. and Wittenberg, U. 2001. Carbon balance of the terrestrial biosphere in the twentieth century: Analyses of CO_2, climate and land use effects with four process-based ecosystem models. *Global Biogeochem. Cycles* **15**, 183–206.

Monsi, M. and Saeki, T. 1953. Über den Lichtfaktor in den Pflanzengesellschaften und seine Bedeutung fur die Stoffproduktion. *Jpn. J. Bot.* **14**, 22–52.

Morimoto, S., Nakazawa, T., Higuchi, K. and Aoki, S. 2000. Latitudinal distribution of atmospheric CO_2 sources and sinks inferred by $\delta^{13}C$ measurements from 1985 to 1991. *J. Geophys. Res.* **105**, 24315–24326.

Myneni, R. B., Nemani, R. R. and Running, S. W. 1997. Estimation of global leaf area index and absorbed per using radiative transfer models. *IEEE Trans. Geosci. Remote Sens.* **35**, 1380–1393.

Nakazawa, T., Morimoto, S., Aoki, S. and Tanaka, M. 1993. Time and space variations of the carbon isotopic ratio of tropospheric carbon dioxide over Japan. *Tellus* **45B**, 257–274.

Nakazawa, T., Ishizawa, M., Higuchi, K. and Trivett, N. B. A. 1997a. Two curve fitting methods applied to CO_2 flask data. *Environmetrics* **8**, 197–218.

Nakazawa, T., Morimoto, S., Aoki, S. and Tanaka, M. 1997b. Temporal and spatial variations of the carbon isotopic ratio of atmospheric carbon dioxide in the western Pacific region. *J. Geophys. Res*. **102**, 1271–1285.

Nemani, R. R. and Running, S. W. 1989. Testing a theoretical climate-soil-leaf area hydrologic equilibrium of forests using satellite data and ecosystem simulation. *Agric. For. Meteorol*. **44**, 245–260.

Nemani, R. R. and Running, S. W. 1996. Global vegetation cover changes from coarse resolution satellite data. *J. Geophys. Res.* **101**, 7145–7162.

Nemry, B., François, L., Gérand, J.-C., Bondeau, A., Heimann, M. and the Potsdam NPP Model Intercomparison. 1999. Comparing global models of terrestrial net primary productivity: analysis of the seasonal atmospheric CO_2 signal. *Global Change Biol.* **5**, Suppl. 1, 65–76.

Potter, C. S., Randerson, J. T., Field, C. B., Matson, P. A., Vitousek, P. M., Mooney, H. A. and Klooster, S. A. 1993. Terrestrial ecosystem production: A process model based on global satellite and surface data. *Global Biogeochem. Cycles* **7**, 811–841.

Ramonet, M. and Monfray, F. 1996. CO_2 baseline concept in 3-D atmospheric transport models. *Tellus* **48B**, 502–520.

Randerson, J. T., Thompson, M. V., Malmstrom, C. M., Field C. B. and Fung, I. Y. 1996. Substrate limitations for heterotrophs: Implications for models that estimate the seasonal cycle of atmospheric CO_2. *Global Biogeochem. Cycles* **10**, 585–602.

Randerson, J. T., Matthew, M. T., Conway, T. J., Fung, I. Y. and Field, C. B. 1997. The contribution of terrestrial sources and sinks to trends in the seasonal cycles of atmospheric carbon dioxide. *Global Biogeochem. Cycles* **11**, 553–560.

Rayner, P. J., Law, R. M. and Dargaville, R. 1999. The relationship between tropical CO_2 fluxes and the El Niño-Southern Oscillation. *Geophys. Res. Lett*. **26**, 493–496.

Rotty, R. M. 1987. Estimates of seasonal variation in fossil fuel CO_2 emissions. *Tellus* **39B**, 184–202.

Running, S. W. 1994. Testing FOREST-BGC ecosystem process simulations across a climatic gradient in Oregon. *Ecol. Appl*. **4**, 238–234.

Running, S. W. and Coughlan, J. C. 1988. A general model of forest ecosystem processes for regional applications. *Ecol. Model.* **42**, 125–154.

Running, S. W. and Hunt, E. R. Jr., 1993. Generalization of a forest ecosystem process model for other biomes, Biome-BGC, and an application for global-scale models. In: *Scaling physiological processes: leaf to globe* (eds. J. R. Ehleringer and C. B. Field). Academic Press, San Diego, Calif., USA., 141–151

Schubert, S., Rood, R. and Pfaendtner, J. 1993. An assimilated dataset for Earth science applications. *Bull. Am. Meteorol. Soc*. **74**, 2331–2342.

Staub, B. and Rosenzweig, C. 1986. Global digital data sets of soil type, soil texture, surface slope, and other properties: Documentation of archived tape data. *Tech. Memo.*, 100685. NASA, Greenbelt, Maryland, USA.

Takahashi, T., Sutherland, S. C., Sweeney, C., Poisson, A., Metzl, N., Tilbrook, B., Bates, N., Wanninkhof, R., Feely, R. A., Sabine, C., Olafsson, J. and Nojiri, Y. 2002. Global sea-air CO_2 flux based on climatological surface ocean pCO_2, and seasonal biological and temperature effects. *Deep Sea Res. II* **49**, 1601–1622.

Thornton, P. E. 1998. Regional ecosystem simulation: combining surface- and satellite-based observations to study linkages between terrestrial energy and mass budgets. Ph.D. Thesis, The University of Montana, Missoula, Montana, USA, 280 pp.

Thornton, P. E., Hasenauer, H. and White, M. A. 2000. Simultaneous estimation of daily solar radiation and humidity from observed temperature and precipitation: an application over complex terrain in Austria. *Agric. For. Meteorol*. **104**, 255–271.

Thornton, P. E., Law, B. E., Gholz, H. L., Clark, K. L., Falge, E., Ellsworth, D. S., Goldstein, A. H., Monson, R. K., Hollinger, D., Falk, M., Chen, J. and Sparks, J. P. 2002. Modeling and measuring the effects of disturbance history and climate on carbon and water budgets in evergreen needleleaf forests. *Agric. For. Meteorol*. **133**, 185–222.

Thornton, P. E. and Running, S. W. 1999. An improved algorithm for estimating incident daily solar radiation from measurements of temperature, humidity, and precipitation. *Agric. For. Meteorol.* **93**, 211–228.

Webb, R. S., Rosenzweig, C. E. and Levine, E. R. 1991. A global data set of soil particle size properties. *Tech. Memo.* 4286. NASA, Greenbelt, Maryland, USA.

WMO WDCGG. 2000. Report No. 21, (ed. Japan Meteorological Agency in cooperation with the WMO), 449 pp.